RSC Advances

PAPER

View Article Online
View Journal | View Issue

Cite this: *RSC Adv.*, 2019, **9**, 19450

Tetrathiafulvalene: effective organic anodic materials for WO_3-based electrochromic devices†

Yong Min Kim,‡[a] Xinlin Li,‡[b] Keon-Woo Kim,[c] Se Hyun Kim *[c] and Hong Chul Moon *[a]

Received 15th April 2019
Accepted 14th June 2019

DOI: 10.1039/c9ra02840d

rsc.li/rsc-advances

Finding a new, effective anodic species is a challenge for achieving simpler low-voltage tungsten trioxide (WO_3)-based electrochromic devices (ECDs). In this work, we utilize tetrathiafulvalene (TTF) and demonstrate its reversible redox behaviors as an electrolyte-soluble anodic species. The concentration of TTF in the electrolyte is varied to optimize device performance. When the TTF concentration is low (0.01 M), a smaller maximum transmittance difference ($\Delta T_{max} \sim 34.2\%$) and coloration efficiency ($\eta \sim 59.6$ cm^2 C^{-1}) are measured. Although a better performance of $\Delta T_{max} \sim 93.7\%$ and $\eta \sim 74.5$ cm^2 C^{-1} is achieved at 0.05 M TTF, the colored state could no longer return to its original form. We conclude that 0.03 M of TTF is the appropriate concentration for high-performance WO_3 ECDs with high optical contrast and reversible EC behaviors. The irreversible EC transition at high concentrations of TTF is attributed to the agglomeration of TTF molecules.

1. Introduction

Electrochromic (EC) materials have attracted considerable attention due to their electric responsive behaviors that change optical absorbance or transmittance.[1–3] EC devices (ECDs) have found relatively new applications such as functional energy storage devices (referred to as EC capacitors; ECSs),[4–6] and electronic skins (e-skins).[7,8] Nonetheless, most applications are in smart windows[9–14] for buildings, cars, sunglasses, and reflective displays.[15–26]

Among the several categories of EC materials, inorganic films are preferred to organic small molecules[15–21] or conducting polymers[22–26] because of their higher photochemical stability.[27–29] Tungsten trioxide (WO_3) is one example of a metal oxide exhibiting reversible EC behaviors.[30–38] Typical WO_3-based ECDs are comprised of two transparent electrodes, a cathodic WO_3 film, an electrolyte, and a secondary anodic EC film. In particular, the secondary anodic films are essential for achieving low-voltage devices. Without them, reductive coloration of WO_3 occurs only when the electrolyte near the anode is decomposed, which greatly degrades device performance.[4,30]

Recently, several efforts have been made to simplify the device structure by directly incorporating the anodic species into the electrolyte.[4,30,31] In this process, the additional deposition of secondary film is unnecessary, and WO_3 ECDs are fabricated straightforwardly. However, possible candidates available for electrolyte-soluble anodic species with high electrochemical stability are limited to hydroquinone (HQ),[4] ferrocene (Fc),[30] and ferrocene derivatives such as dimethyl Fc (dmFc).[31] Therefore, the discovery of new anodic candidates and their successful applications are a challenge for high-performance, simple WO_3 ECDs.

Herein, tetrathiafulvalene (TTF)-containing electrolytes were prepared and used in ECDs based on WO_3. As an electrolyte-soluble anodic material, we selected and evaluated TTF that is an electron-donor with outstanding redox properties.[39,40] The redox potential of TTF is more negative than that of representative anodic species, Fc. This implies that WO_3 ECDs will be able to operate at very low voltages when combined with TTF. We varied the concentration of TTF in the electrolyte to investigate the correlation between TTF concentration and device performance. Irrespective of TTF content, noticeable changes in the absorption spectra were observed at −0.3 V. However, other characteristics including maximum transmittance contrast (ΔT_{max}), response time (Δt), and coloration efficiency depended on TTF concentration. For example, ΔT_{max} and coloration efficiency were small and kinetic response was relatively slow at low TTF concentration (*e.g.* 0.01 M), due to the concentration imbalance between anodic (TTF) and cathodic (WO_3) materials. These properties were improved as the TTF concentration increased. However, TTF agglomerates were formed when the TTF concentration reached 0.05 M, which prevented the colored WO_3 film from returning to its original transparent state. Our results demonstrate that TTF can successfully serve as an electrolyte-soluble anodic species, although the appropriate concentration of TTF is important for achieving a balanced, high-performance WO_3 ECDs.

[a]*Department of Chemical Engineering, University of Seoul, Seoul 02504, Republic of Korea. E-mail: hcmoon@uos.ac.kr*

[b]*College of Electromechanical Engineering, Qingdao University, Qingdao 266071, China*

[c]*School of Chemical Engineering, Yeungnam University, Gyeongsan, North Gyeongsang 38541, Republic of Korea. E-mail: shkim@ynu.ac.kr*

† Electronic supplementary information (ESI) available. See DOI: 10.1039/c9ra02840d

‡ These authors contributed equally to this work.

2. Experimental

All chemicals used in this work were purchased from Sigma-Aldrich. ITO-coated glasses (sheet resistance: 10 Ω sq^{-1}, Asahi Glass Co.) were sequentially cleaned with acetone (20 min) and DI-water (20 min) under sonication followed by UV/ozone treatment for 10 min before use. EC WO_3 film was prepared on an indium tin oxide (ITO)-coated glass by a low-temperature sol–gel process. The detailed synthetic process is described elsewhere.[31] A propylene carbonate (PC) solution containing 0.5 M $LiClO_4$ (supporting electrolyte) and TTF (anodic material) was employed for an electrolyte layer, in which the concentration of TTF was varied (*i.e.* 0.01, 0.03, and 0.05 M).

EC devices (ECDs) based on WO_3 and TTF-containing electrolytes were fabricated straightforwardly. First, a gasket (thickness of 60 μm) serving as a spacer was placed on the WO_3-coated ITO electrode, and the electrolyte solution filled around the gasket. The dimension of active area was 25 mm × 25 mm (width × length). Next, the counter ITO electrode was assembled on the gasket, followed by complete sealing using silicon resin.

Cyclic voltammograms of TTF were obtained using a potentiostat (Weis 500, WonA Tech.) to investigate its redox behaviors. Changes in optical characteristics at different voltages were recorded on a UV-vis spectrometer (GENESYS 10S, Thermo Scientific™), where DC voltage input was suppled from a source meter (Keithley 2400, Tektronix). Time-dependent transmittance profiles during coloration and bleaching were obtained using the same instrumentations. All photographs for analyzing agglomeration behaviors of TTF after ECD operation were taken using an optical microscopy (OM, Nikon Eclipse LV100ND). Ionic conductivity of the TTF containing electrolyte was determined by electrochemical impedance spectrometry (EIS) (IM6, ZAHNER) at a frequency range of 10^{-1} to 10^{6} Hz with AC amplitude of 10 mV. Noted that electrolyte layers containing TTF were highly conductive. For example, the ionic conductivity of ~5.4 mS cm^{-1} at 25 °C was measured for 0.03 M TTF-containing electrolyte (see Fig. S1 in the ESI†).

3. Results and discussion

Fig. 1 displays the structure of the WO_3 ECDs with electrolytes that contain the TTF anodic species as well as the overall electrochemical coloration reactions. Similar to previously reported

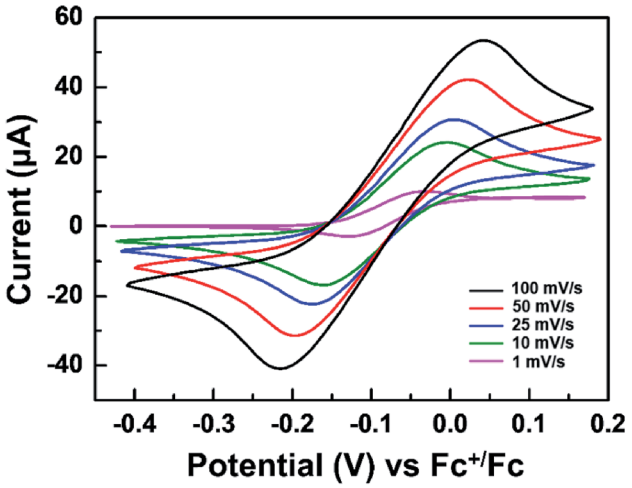

Fig. 2 Cyclic voltammograms (CV) of tetrathiafulvalene (TTF) at various scan rates. 10 mM TTF was dissolved in a propylene carbonate (PC) solution containing 0.1 M tetrabutylammonium hexafluorophosphate ($TBAPF_6$), where a platinum disk, Ag wire, and ITO-coated glass were employed as the working, reference and counter electrode, respectively. Ferrocene (Fc) was used as an internal standard.

anodic materials,[4,30,31] the use of TTF further simplifies the device with the absence of anodic films on the counter electrode; the fabrication is more convenient and straightforward. When a negative bias is applied to the WO_3-coated electrode (cathode, working electrode), the WO_3 layer is reduced to colored $Li_xW_{1-x}^{6+}W_x^{5+}O_3$ with incorporating Li^+ ions.[38] Simultaneously, the TTF dissolved in the electrolyte is oxidized to $TTF^{+\bullet}$ near the counter ITO electrode (anode, counter electrode). It should be noted that this work first employed the redox pair of TTF (anodic species) and WO_3 (cathodic EC material). Although there is a paper in which TTF was utilized as an anodic material, a different EC chromophore (ethyl viologen, EV) was introduced.[41] The WO_3/TTF system in this work showed lower coloration voltage and larger maximum transmittance contrast compared to the ECDs with EV/TTF. These features will be analyzed shortly.

Before characterizing the ECD performance, we evaluated the feasibility of TTF as an electrolyte-soluble anodic species for WO_3 ECDs. The requirements for counter anodic materials should include stable redox behaviors and appropriate redox potential. Fig. 2 shows cyclic voltammograms of TTF in a PC

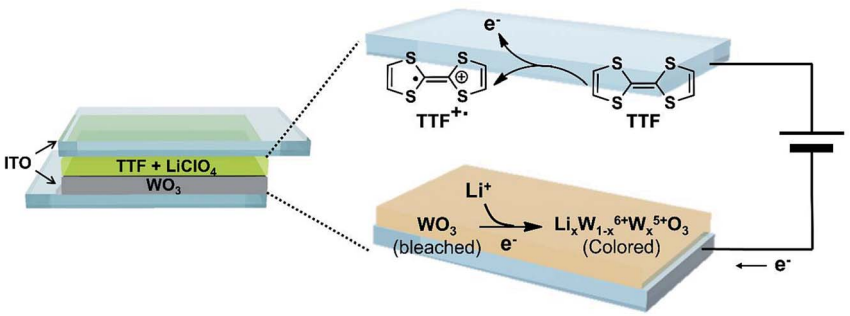

Fig. 1 Schematic illustration and reaction diagram of the coloration process for ECDs in this work.

solution. The redox reaction of the $TTF^{+\bullet}$/TTF pair was quite reversible regardless of scan rate. Comparable cathodic (i_{pc}) and anodic peak currents (i_{pa}) indicate high reversibility of redox couple $TTF^{+\bullet}$/TTF. For example, $i_{pc}/i_{pa} \sim 0.99$ was extracted at 25 mV s^{-1}. Another notable feature of TTF is more negative redox potential compared to previously reported anodic materials such as Fc or dmFc. In general, the coloration voltage is determined by the redox potential difference between the cathodic and anodic species. Because WO_3 is a cathodic EC material, a lower voltage operation is expected when using TTF oxidized at −0.075 V *vs.* Fc^+/Fc (see Fig. 2). We extracted diffusion coefficients (D) of TTF and TTF^+ using Randles–Sevcik equation (see Fig. S2 in the ESI†). As a result, the D_{TTF} and D_{TTF^+} were determined to be $\sim 6.28 \times 10^{-7}$ and $\sim 4.69 \times 10^{-7}$ cm^2 s^{-1}, respectively.

It is noted that the shape of active areas can be conveniently adjusted if we utilize gel electrolytes containing TTF, although in this work we focus on the effect of TTF in the liquid electrolyte on device performance. For example, when the high toughness gel based on poly(vinylidene fluoride-*co*-hexafluoropropylene) (PVDF-*co*-HFP) was employed, the ECDs were demonstrated through 'cut-and-stick' strategy (see Fig. S3 in the

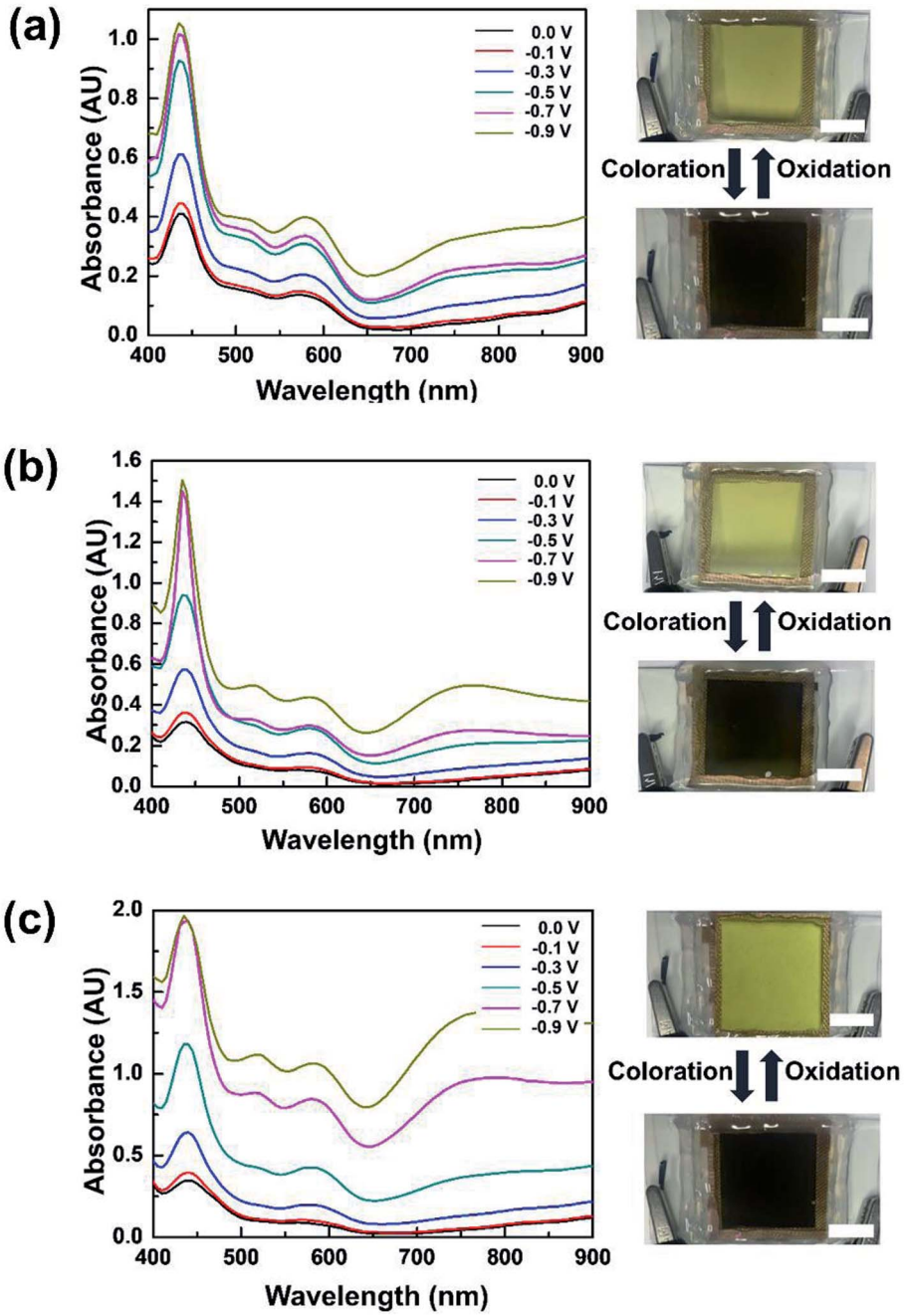

Fig. 3 Voltage dependence of UV-vis absorbance spectra at various TTF concentrations: (a) 0.01 M (b) 0.03 M (c) 0.05 M. Photographs display corresponding bleached (no bias) and colored states (−0.9 V). The scale bar represents 10 mm.

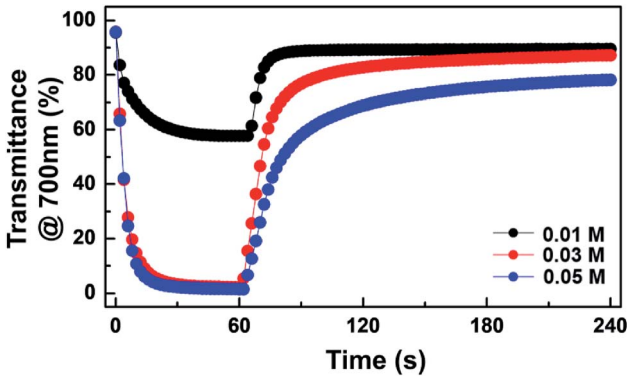

Fig. 4 Transient transmittance profiles at 700 nm for ECDs at various TTF concentrations upon application of −0.9 V (coloration) followed by bleaching under short-circuit condition.

ESI†).[19,42–44] We also expect that the fabrication of large area devices is available by taking advantage of solution processability (*e.g.* spin coating) of gel electrolytes.

The dependence of optical characteristics on applied voltages was investigated at three TTF concentrations (Fig. 3). When 0.01 M TTF was included in the electrolyte, a noticeable change in absorption spectra was observed at −0.3 V (Fig. 3a). This coloration voltage is obviously lower than those of previous WO_3 ECDs including electrolyte-soluble anodic species,[4,30,31] which is attributed to the lower redox potential of TTF. As the applied voltage increased, stronger absorption appeared over the entire experimental wavelength. Photographs also indicate remarkable differences in color between bleached and colored states (Fig. 3a). Similar EC behaviors were observed at 0.03 and 0.05 M TTF (see Fig. 3b and c, respectively). However, device response at a higher TTF content was more sensitive to external voltage changes. In addition, we investigated thermal stability of the WO_3 ECD including TTF, for which the device was exposed to 80 °C for 1 h. There was no noticeable change in both bleached and colored states. This result indicates the high thermal stability of TTF-containing WO_3 ECDs (Fig. S4 in the ESI†).

Device dynamics under consecutive coloration and bleaching are recorded in Fig. 4. EC behaviors of the device with 0.01 M TTF were reversible, but a maximum transmittance contrast (ΔT_{max}) was only ~34.2%. The coloration (Δt_c) and bleaching time (Δt_b) were ~24 s and ~10 s, respectively. It is noted that the response time (Δt) was determined as the time at which 90% of ΔT_{max} was achieved. A significant enhancement in ΔT_{max} was observed as the TTF concentration increased. For example, ΔT_{max} of ~93.0% was achieved at 0.03 M TTF concentration. This improvement originates from the balanced oxidation and reduction reactions near the anode and WO_3-deposited cathode, respectively. In addition, Δt_c (~12 s) at 0.03 M TTF was much faster than at 0.01 M, although bleaching required a longer time to recover. A large ΔT_{max} and fast coloration were also detected at a TTF concentration of 0.05 M, but bleaching was delayed considerably, and the device could not return to the initial state once colored.

The TTF concentration of coloration efficiency (η) was examined. The η value, which is the ratio between variations in optical density (ΔOD) and injected charge (ΔQ), was calculated from the slope of the linear fits in Fig. 5. A higher η was calculated from devices with a larger amount of TTF. For example, while $\eta \sim 74.5$ cm^2 C^{-1} was evaluated at 0.05 M TTF, the ECD with 0.01 M TTF was only ~59.6 cm^2 C^{-1}. This observation can be explained by simultaneous electrochemical reactions of a large number of redox species. In addition, the coloration values are comparable (or higher) to those of ECDs based on WO_3 EC films with other anodic materials (*e.g.* HQ ~ 61.9 cm^2 C^{-1},[4] Fc ~ 34.3 cm^2 C^{-1},[30] and dmFc ~ 60.2 cm^2 C^{-1}

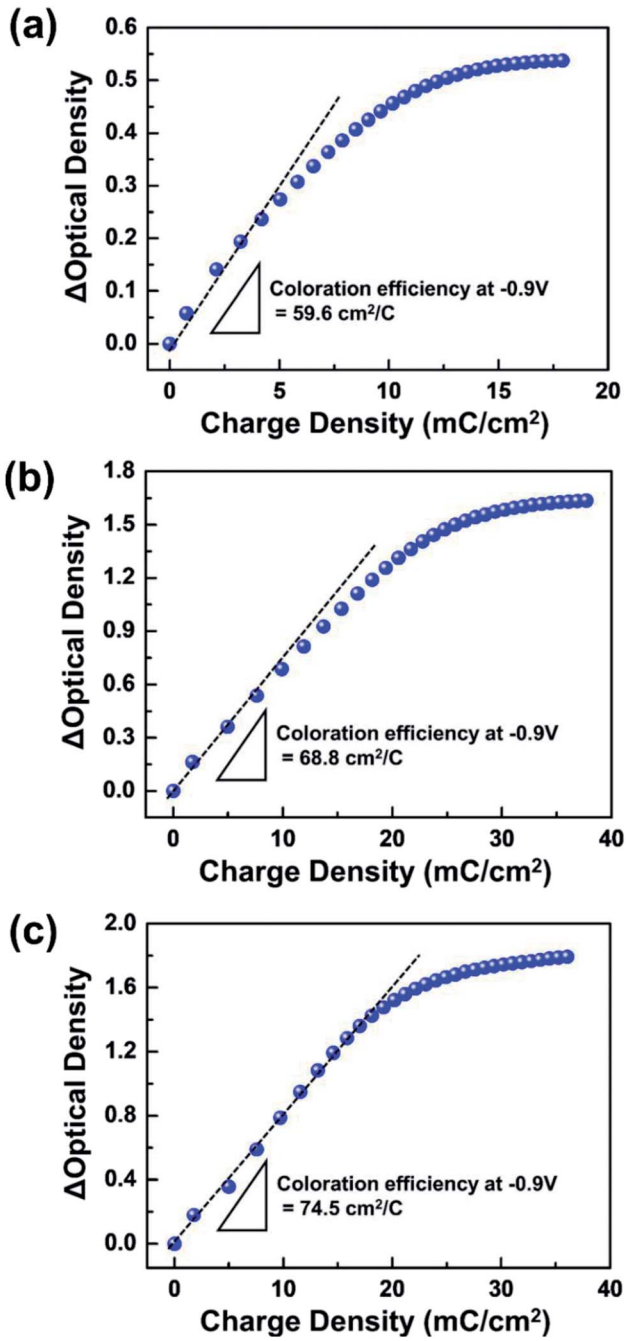

Fig. 5 Dependence of optical density (OD) on the injected charge density at various TTF concentrations in electrolytes: (a) 0.01 M, (b) 0.03 M, and (c) 0.05 M.

Table 1 Summarized EC performance at the three TTF concentrations

TTF concentration (M)	ΔT_{max} (%)	Δt_c (s)	Δt_b (s)	η (cm^2 C^{-1})
0.01	34.2	~24	~10	59.6
0.03	93.0	~12	~28	68.8
0.05	93.7	~10	~68	74.5

(ref. 31)). Accordingly, we conclude that TTF can successfully serve as an efficient anodic material for WO_3 ECDs. The ECD performance at various TTF concentrations is summarized in Table 1.

A remarkable difference in optical characteristics, quicker response, and higher efficiency were realized at 0.05 M TTF. Nonetheless, this concentration cannot be considered optimal for practical applications due to the lack of reversibility (see Fig. 4). We revealed the origin of this performance deterioration

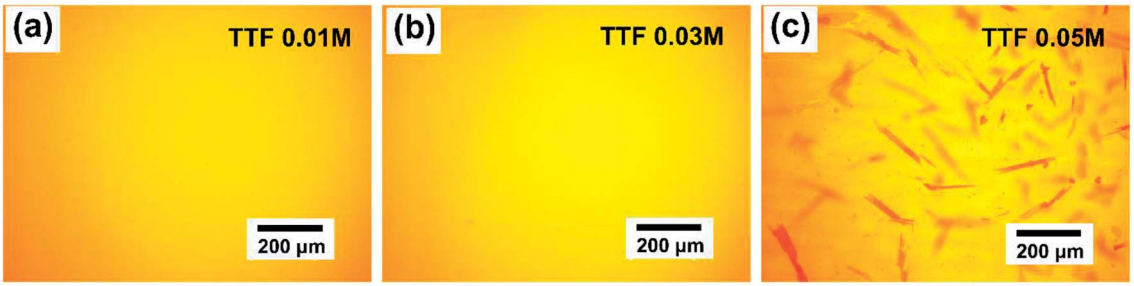

Fig. 6 Optical microscopic photographs for electrolyte layers of ECDs after 100 consecutive coloration/bleaching cycles at various TTF concentrations: (a) 0.01 M, (b) 0.03 M, and (c) 0.05 M.

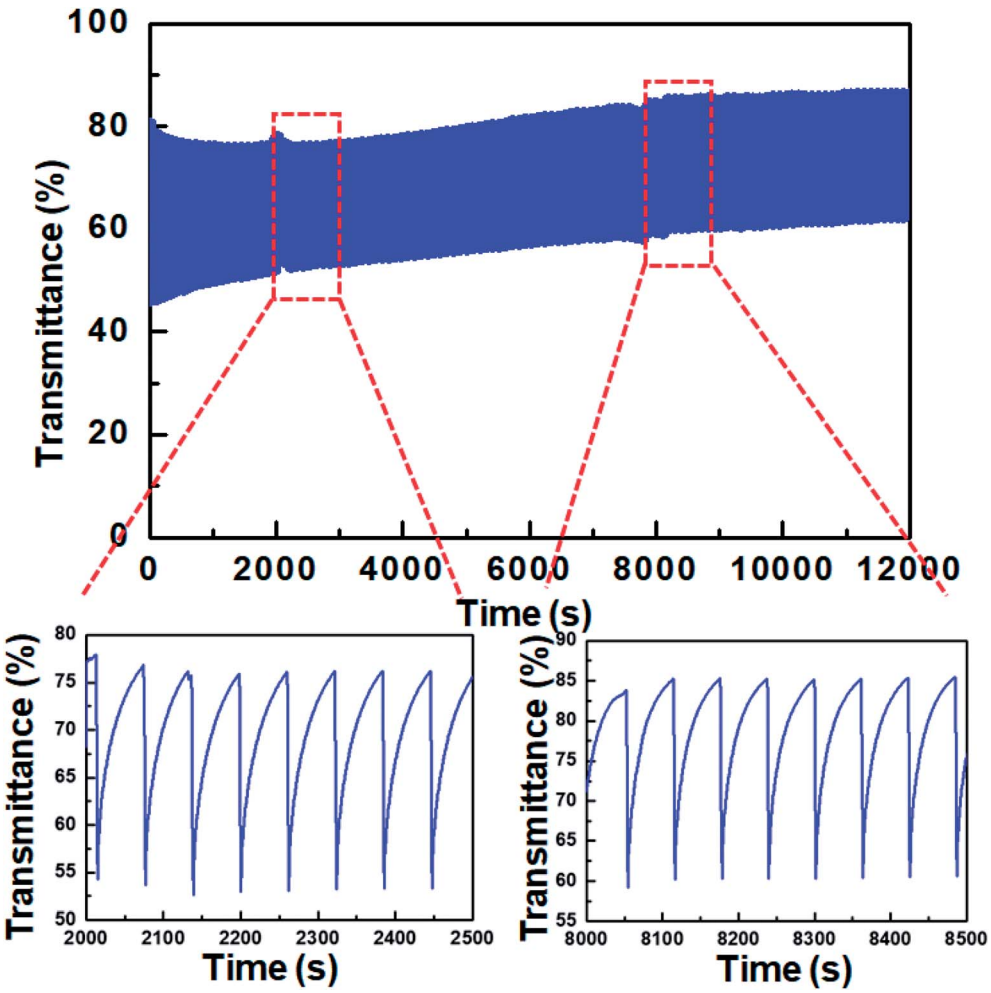

Fig. 7 Variation of transmittance at 700 nm for the WO_3 ECD containing 0.03 M TTF during coloration/bleaching cyclic test.

at a large amount of TTF in the electrolyte. Fig. 6 displays optical microscopic images of TTF-containing electrolyte layer after 100 consecutive coloration/bleaching transitions. A homogeneous phase was maintained at TTF concentrations where reversible transitions of ECDs were shown (see Fig. 6a, b and S5 in the ESI†). On the other hand, a significant aggregation of TTF molecules was detected when the TTF concentration was higher (Fig. 6c). Electrochemical reactions of solid-state redox species occur only near the surface,[45,46] which seriously retards coloration and bleaching and induces irreversible behaviors of ECDs. Therefore, the appropriate TTF concentration (in this case, 0.03 M) is very important for realizing high-performance WO_3 ECDs.

The characterization of coloration/bleaching cyclic stability is essential for evaluating the practical feasibility of ECDs. Accordingly, we assessed the cyclic stability of devices based on WO_3 and TTF. An asymmetric square wave consisting of -0.9 V for 5 s (coloration) and 0.0 V for 55 s (bleaching) was applied, with the consideration of the longer bleaching response. The transmittance was reversibly changed according to the applied voltage over 200 cycles (Fig. 7), implying good cyclic stability of WO_3 ECDs including TTF.

4. Conclusions

In this work, TTF was directly dissolved in the electrolyte and served as the anodic species for WO_3-based ECDs. Electrochemical characteristics of TTF were investigated through CV experiments, which revealed good reversibility of redox reactions of TTF. In addition, a redox potential of TTF lower than those of other electrolyte-soluble anodic materials such as Fc and dmFc was measured. As a result, low-voltage WO_3 ECDs (*e.g.* coloration voltage ~ -0.3 V) were fabricated with TTF-containing electrolytes. We examined effects of TTF concentrations on the device performance. When a low concentration of TTF was employed, the coloration of WO_3 layer was insufficient. On the other hand, at a concentration of 0.05 M TTF, the ECD exhibited a larger transmittance difference between colored and bleached states, faster coloration, and higher coloration efficiency. However, the device could not return to its original state due to the TTF aggregates interfering with proper electrochemical reactions. Overall, these results imply that TTF can be a promising electrolyte-soluble anodic species for high-performance WO_3 ECDs, when the appropriate concentration of TTF is employed.

Conflicts of interest

The authors declare no conflicts of interest.

Acknowledgements

This research was supported by X-mind Corps program of National Research Foundation of Korea (NRF) funded by the Ministry of Science, ICT (NRF-2017H1D8A1030582). This research was supported by "Human Resources Program in Energy Technology" of the Korea Institute of Energy Technology Evaluation and Planning (KETEP), granted financial resource from the Ministry of Trade, Industry and Energy, Republic of Korea (No. 20174030201760).

Notes and references

1 P. M. S. Monk, *The Viologens: Physicochemical Properties, Synthesis and Applications of the Salts of 4,4'-Bipyridine*, J. Wiley & Sons, Chichester, UK, 1998.
2 P. M. S. Monk, R. J. Mortimer and D. R. Rosseinsky, *Electrochromism: Fundamentals and Applications*, VCH, Weinheim, 1995.
3 R. J. Mortimer, *Chem. Soc. Rev.*, 1997, **26**, 147–156.
4 T. Y. Yun, X. Li, S. H. Kim and H. C. Moon, *ACS Appl. Mater. Interfaces*, 2018, **10**, 43993–43999.
5 Y. Kim, M. Han, J. Kim and E. Kim, *Energy Environ. Sci.*, 2018, **11**, 2124–2133.
6 M. Zhu, Y. Huang, Y. Huang, W. Meng, Q. Gong, G. Li and C. Zhi, *J. Mater. Chem. A*, 2015, **3**, 21321–21327.
7 H. H. Chou, A. Nguyen, A. Chortos, J. W. F. To, C. Lu, J. Mei, T. Kurosawa, W. G. Bae, J. B.-H. Tok and Z. Bao, *Nat. Commun.*, 2015, **6**, 8011.
8 H. Park, D. S. Kim, S. Y. Hong, C. Kim, J. Y. Yun, S. Y. Oh, S. W. Jin, Y. R. Jeong, G. T. Kim and J. S. Ha, *Nanoscale*, 2017, **9**, 7631–7640.
9 S. Zhang, S. Cao, T. Zhang, A. Fisher and J. Y. Lee, *Energy Environ. Sci.*, 2018, **11**, 2884–2892.
10 S. Lin, X. Bai, H. Wang, H. Wang, J. Song, K. Huang, C. Wang, N. Wang, B. Li, M. Lei and H. Wu, *Adv. Mater.*, 2017, **29**, 1703238.
11 G. Cai, P. Darmawan, X. Cheng and P. S. Lee, *Adv. Energy Mater.*, 2017, **7**, 1602598.
12 S. Poongodi, P. S. Kumar, Y. Masuda, D. Mangalaraj, N. Ponpandian, C. Viswanathan and S. Ramakrishna, *RSC Adv.*, 2015, **5**, 96416–96427.
13 Z. Wang, M. Zhu, S. Gou, Z. Pang, Y. Wang, Y. Su, Y. Huang, Q. Weng, O. G. Schmidt and J. Xu, *ACS Appl. Mater. Interfaces*, 2018, **10**, 31697–31703.
14 K. Mallikarjuna and H. Kim, *ACS Appl. Mater. Interfaces*, 2019, **11**, 1969–1978.
15 H. C. Moon, T. P. Lodge and C. D. Frisbie, *Chem. Mater.*, 2015, **27**, 1420–1425.
16 H. C. Lu, S. Y. Kao, T. H. Chang, C. W. Kung and K. C. Ho, *Sol. Energy Mater. Sol. Cells*, 2016, **147**, 75–84.
17 J. H. Huang, C. Y. Yang, C. Y. Hsu, C. L. Chen, L. Y. Lin, R. R. Wang, K. C. Ho and C. W. Chu, *ACS Appl. Mater. Interfaces*, 2009, **1**, 2821–2828.
18 G. J. Stec, A. Lauchner, Y. Cui, P. Nordlander and N. J. Halas, *ACS Nano*, 2017, **11**, 3254–3261.
19 H. Oh, D. G. Seo, T. Y. Yun, S. B. Lee and H. C. Moon, *Org. Electron.*, 2017, **51**, 490–495.
20 H. Oh, D. G. Seo, T. Y. Yun, C. Y. Kim and H. C Moon, *ACS Appl. Mater. Interfaces*, 2017, **9**, 7658–7665.
21 K.-W. Kim, H. Oh, J. H. Bae, H. Kim, H. C. Moon and S. H. Kim, *ACS Appl. Mater. Interfaces*, 2017, **9**, 18994–19000.
22 D. G. Seo and H. C. Moon, *Adv. Funct. Mater.*, 2018, **28**, 1706948.

23 W. Lu, A. G. Fadeev, B. Qi and B. R. Mattes, *J. Electrochem. Soc.*, 2004, **151**, H33–H39.
24 H. W. Heuer, R. Wehrmann and S. Kirchmeyer, *Adv. Funct. Mater.*, 2002, **12**, 89–94.
25 S. A. Sapp, G. A. Sotzing, J. L. Reddinger and J. R. Reynolds, *Adv. Mater.*, 1996, **8**, 808–811.
26 B. C. Thompson, P. Schottland, K. Zong and J. R. Reynolds, *Chem. Mater.*, 2000, **12**, 1563–1571.
27 A. F. Akbulatov, S. Y. Luchkin, L. A. Frolova, N. N. Dremova, K. L. Gerasimov, I. S. Zhidkov, D. V. Anokhin, E. Z. Kurmaev, K. J. Stevenson and P. A. Troshin, *J. Phys. Chem. Lett.*, 2017, **8**, 1211–1218.
28 W. Guo, J. J. Li, A. Wang and X. Peng, *J. Am. Chem. Soc.*, 2003, **125**, 3901–3909.
29 X. Shen, L. Zhu, C. Huang, H. Tang, Z. Yu and F. Deng, *J. Mater. Chem.*, 2009, **19**, 4843–4851.
30 J. Bae, H. Kim, H. C. Moon and S. H. Kim, *J. Mater. Chem. C*, 2016, **4**, 10887–10892.
31 J. Bae, D. G. Seo, S. M. Park, K. T. Park, H. Kim, H. C. Moon and S. H. Kim, *J. Phys. D: Appl. Phys.*, 2017, **50**, 465105.
32 C. Yan, W. Kang, J. Wang, M. Cui, X. Wang, C. Y. Foo, K. J. Chee and P. S. Lee, *ACS Nano*, 2014, **8**, 316–322.
33 J. Wang, E. Khoo, P. S. Lee and J. Ma, *J. Phys. Chem. C*, 2008, **112**, 14306–14312.
34 L. Xiao, Y. Lv, W. Dong, N. Zhang and X. Liu, *ACS Appl. Mater. Interfaces*, 2016, **8**, 27107–27114.
35 G. Cai, M. Cui, V. Kumar, P. Darmawan, J. Wang, X. Wang, A. L.-S. Eh, K. Qian and P. S. Lee, *Chem. Sci.*, 2016, **7**, 1373–1382.
36 J. Zhang, J. P. Tu, D. Zhang, Y. Q. Qiao, X. H. Xia, X. L. Wang and C. D. Gu, *J. Mater. Chem.*, 2011, **21**, 17316–17324.
37 G. F. Cai, D. Zhou, Q. Q. Xiong, J. H. Zhang, X. L. Wang, C. D. Gu and J. P. Tu, *Sol. Energy Mater. Sol. Cells*, 2013, **117**, 231–238.
38 T. Y. Yun, X. Li, J. Bae, S. H. Kim and H. C. Moon, *Mater. Des.*, 2019, **162**, 45–51.
39 M. Bendikov and F. Wudl, *Chem. Rev.*, 2004, **104**, 4891–4945.
40 N. Martín, *Chem. Commun.*, 2013, **49**, 7025–7027.
41 S. Mishra, P. Yogi, S. K. Saxena, S. Roy, P. R. Sagdeo and R. Kumar, *J. Mater. Chem. C*, 2017, **5**, 9504–9512.
42 K. H. Lee, M. S. Kang, S. Zhang, Y. Gu, T. P. Lodge and C. D. Frisbie, *Adv. Mater.*, 2012, **24**, 4457–4462.
43 H. C. Moon, T. P. Lodge and C. D. Frisbie, *J. Mater. Chem. C*, 2016, **4**, 8448–8453.
44 T. Y. Yun and H. C. Moon, *Org. Electron.*, 2018, **56**, 178–185.
45 Y. Alesanco, A. Viñuales, J. Rodriguez and R. Tena-Zaera, *Materials*, 2018, **11**, 414.
46 A. A. Argun, P.-H. Aubert, B. C. Thompson, I. Schwendeman, C. L. Gaupp, J. Hwang, N. J. Pinto, D. B. Tanner, A. G. MacDiarmid and J. R. Reynolds, *Chem. Mater.*, 2004, **16**, 4401–4412.